

# Anisotropy and asymmetry in fully developed turbulence

S. I. Vainshtein

*Department of Astronomy and Astrophysics, University of Chicago*

## Abstract

Using experimental longitudinal and transverse velocities data for very high Reynolds number turbulence, we study both anisotropy and asymmetry of turbulence. These both seem to be related to small scale turbulent structures, and to intermittency. We may assume that the large scale velocity shear gives an impact into the small scale turbulence, resulting in non-locality, and related anomalous events.

## INTRODUCTION

Recently considerable attention has been devoted to the study of local isotropy of the high Reynolds number turbulence suggested by [1]. The turbulence is stirred at the large scales, and this energy is transported into the small scales, where, after intense nonlinear interaction, it becomes isotropic. Deviation from isotropy would mean that there is direct interaction between large scales containing non-universal anisotropy and small scales, leading to non-universal behavior of small scale spectral properties.

It was indeed shown experimentally that in a sheared turbulence the isotropy is not sufficiently restored for both scalar and velocity fields, see [2], [3], [4], [5], [6], [7], [8].

High Reynolds number (atmospheric) turbulence also shows deviations from isotropy. It was shown that the large scale shear does contribute into the scaling of the structure functions, see [9]. Anisotropic scaling of high-order structure functions was studied by [10]. It was shown that the anisotropy in small scales remains stronger than expected before. The SO(3) decomposition was used to describe the anisotropy, see [10], [11], [12], [13]. The persistent anisotropy in small scale turbulence was found to be related to the intermittency corrections, [14].

In numerical simulations, the failure to return to isotropy was linked to both asymmetry of the probability distribution function (PDF) and to the vortex sheets, [15]. It became clear that the shear in the integral scale induces asymmetry down to the small scales, where it is manifested by intermittent structures like cliffs, etc., [16].

On the other hand, the asymmetry PDF was found to be related to the intermittency, [17]. Thus, these three items, i.e., anisotropy, asymmetry and intermittency seem to be related. Note, however, that, in principle, these items are independent of each other. For example, the asymmetry of the PDF appears naturally in turbulence, even without any anisotropy. Denote  $u$  - longitudinal and  $v$  - transverse (vertical) components of the velocity, and  $u_r = u(x+r) - u(x)$ ,  $v_r = v(x+r) - v(x)$ , the velocity increments. Then, we have,

$$\langle u_r \rangle = 0, \quad \text{and} \quad \langle v_r \rangle = 0, \quad (1)$$

and (in inertial range)

$$\langle u_r^3 \rangle = -\frac{4}{5}\varepsilon r, \quad (2)$$

the so-called 4/5-Kolmogorov law [18]. Besides,

$$\langle u_r v_r^2 \rangle = \frac{1}{6} \frac{d\langle u_r^3 \rangle}{dr}, \quad (3)$$

[19], [20]. The fact that the first moments vanish, see (1), whereas the two third moments (2) and (3) do not clearly indicate that both the PDF for  $u_r$  and the joint PDF for  $u_r$  and  $v_r$  are asymmetric.

As the Kolmogorov law is derived assuming isotropic turbulence, this asymmetry in principle exists without anisotropy. Besides, the scaling defined by the Kolmogorov law (2) does not have any intermittency corrections. Nevertheless, as mentioned above, the asymmetry (even without anisotropy) may be related to the intermittency of turbulence, as suggested by [17], [21] and [22]. Still, this connection does not seem to present the whole picture. Presumably, as in sheared flows, the anisotropy should also be taken into considerations. As mentioned above, even very high-Reynolds-number turbulence manifests anisotropy in small scales, which is higher than predicted from dimensional arguments by [23]. This suggests that there is additional to Kolmogorov cascade transfer of energy from large scales directly to small, leading to anomalous events like intermittency and anisotropy.

In this paper we focus on these events. In particular, we construct experimental joint PDF for  $u_r$  and  $v_r$  to see directly if anisotropy and asymmetry is present in rare violent events (responsible for the intermittency). Note that constructing the joint 2D PDF's proved to be useful in turbulence, see for example [24], [25], [26]. Even more information about the connection between anisotropy, asymmetry and intermittency we obtain from several conditional and cumulative averages described in the next section.

## PROBLEM DESCRIPTION

We will work with dimensionless variables,

$$u'_r = \frac{u_r}{\langle u_r^2 \rangle^{1/2}}, \quad v'_r = \frac{v_r}{\langle v_r^2 \rangle^{1/2}},$$

and construct experimental joint PDF,  $p(u'_r, v'_r)$  to study both asymmetry and anisotropy. This 2D distribution is useful to compare with 2D Gaussian anisotropic distribution,  $p_G$ , see Appendix, (15), (16).

The joint 2D PDF gives general information about the distribution. More detailed information which is easier to analyze are provided by different 1D distributions and cumulative

moments. In particular, we are interested in studding the third mixed moment, (3),

$$\langle u_r v_r^2 \rangle = \int u_r v_r^2 p(u_r, v_r) du_r dv_r, \quad (4)$$

that is, it is important to find out what part of the distribution contributes most into this moment. It was shown before, see [27], that the tail parts of 1D distributions satisfactory recover the moment.

Additional information is given by conditional average,

$$\langle v_r^2 | u_r \rangle = \int v_r^2 p(v_r | u_r) dv_r = \frac{\int v_r^2 p(v_r, u_r) dv_r}{p(u_r)} = \frac{\Phi(u_r)}{p(u_r)}, \quad (5)$$

or, in dimensionless variables,

$$\langle v_r'^2 | u_r' \rangle = \int p(v_r' | u_r') v_r'^2 dv_r' = \frac{\Phi(u_r')}{p(u_r')}. \quad (6)$$

In these expressions we introduced

$$\Phi(u_r) = \int v_r^2 p(u_r, v_r) dv_r, \quad \Phi(u_r') = \int v_r'^2 p(u_r', v_r') dv_r' \quad (7)$$

Therefore,

$$\langle u_r v_r^2 \rangle = \int u_r \langle v_r^2 | u_r \rangle p(u_r) du_r = \int u_r \Phi(u_r) du_r, \quad (8)$$

$$\langle u_r' v_r'^2 \rangle = k_a = \int u_r' \langle v_r'^2 | u_r' \rangle p(u_r') du_r' = \int u_r' \Phi(u_r') du_r' \quad (9)$$

The function  $\Phi(u_r)$  deserves special attention. It follows from (7) that

$$\int \Phi(u_r) du_r = \langle v_r^2 \rangle, \quad (10)$$

that is, in a way, the function is a  $v_r^2$ -distribution versus  $u_r$ . The first moment of this distribution should not vanish, as it follows from (8). This means that the  $v_r^2$ -distribution should be asymmetric. For Gaussian distribution, the function  $\Phi_G$  can be easily calculated, see Appendix, (18).

We used x-wire data acquired at Brookhaven National Lab. Distance of probe above the ground: 35m; Number of samples: 40960000 per component, that is, for longitudinal ( $u$ ) and transverse ( $v$ ) components. Sampling frequency: 5 kHz. Mean velocity: 5.15076224 m/s; rms  $u$ -velocity: 1.81617371 m/s; rms  $v$ -velocity: 1.3646025 m/s; Taylor Reynolds number: 10680 (courtesy of Sreenivasan). As usual, the data are interpreted using the Taylor's hypothesis.

All throughout the paper we process data for closest two samples, that is,  $r$  corresponds to the smallest distance between two samples.

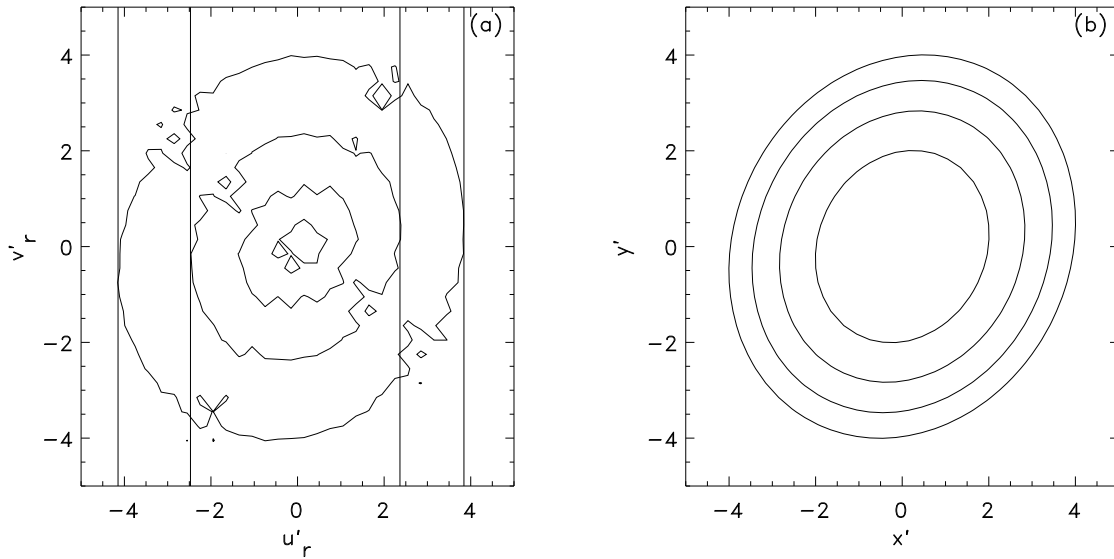


FIG. 1: Experimental joint PDF, core part. The indicated levels correspond to  $e^{-2}$ ,  $e^{-4}$ ,  $e^{-6}$ ,  $e^{-8}$  of the maximum of the PDF, inside out correspondingly. The contours a) depict experimental PDF, and b) – Gaussian anisotropic (16).

## JOINT PDF

Figures 1 and 2 present this PDF in different ranges. We (loosely) define these regions as core part, Fig. 1, and tail part, Fig. 2. Clearly, Fig. 1 corresponds to the main events, while Fig. 2 - to the rare and violent events, – as indicated by the levels given in the captures.

It is clear that the main events, Fig. 1, are not much different from Gaussian. Both PDF's are noticeably anisotropic, that is the levels are roughly ellipses with big axes inclined at some angles to the x-axis. The positions of the levels are roughly the same. The only difference is asymmetry, the latter being absent in the Gaussian PDF by construction.

The asymmetry of the experimental PDF is evident from the following observations. The left edge of the outer level is at  $u'_r = -4.1$ , while the right edge of it is at  $u'_r = 3.8$ ; the left edge of the next level is at  $u'_r = -2.5$ , while the right edge is at  $u'_r = 2.4$ .

Note that both anisotropy and asymmetry are expected to be manifested by the main events.

Consider now Fig. 2. We note first that now there is dramatic difference between the

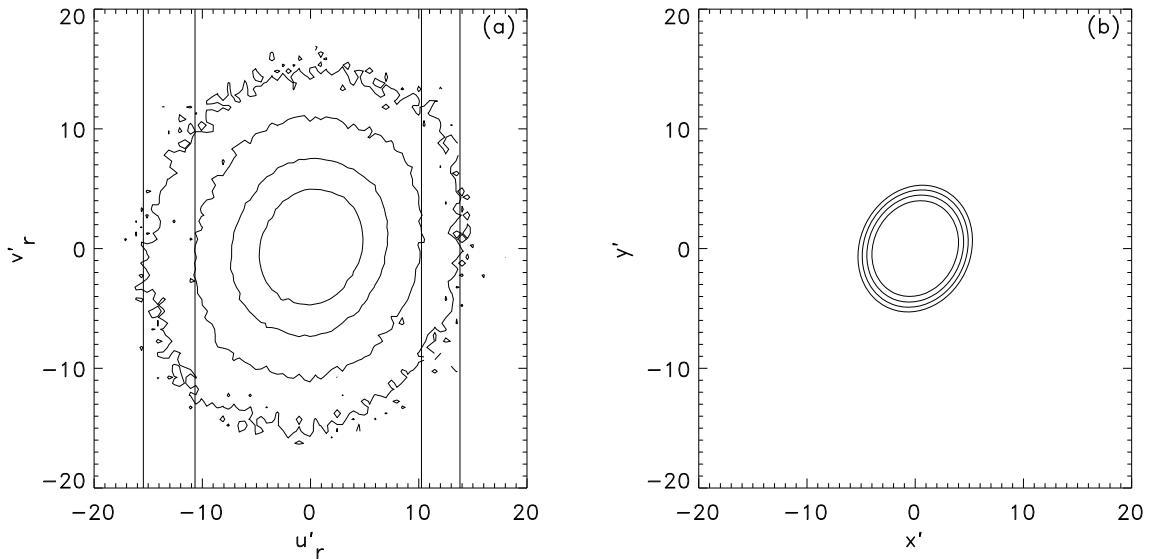


FIG. 2: Experimental joint PDF, tail part. The indicated levels correspond to  $e^{-8}$ ,  $e^{-10}$ ,  $e^{-12}$ ,  $e^{-14}$  of the maximum of the PDF, inside out correspondingly. The contours a) depict experimental PDF, and b) – Gaussian anisotropic (16).

experimental contours and Gaussian. Namely, the experimental contours are much further away from the core values than the corresponding Gaussian. This feature is however anticipated, simply corresponding to the presence of tails, that is, to intermittency – in both longitudinal and transverse velocity component increments.

On the other hand, other features of the rare events PDF are more surprising. The experimental contours in the Fig. 2(a) look roughly similar to those in Fig. 1(a), only rescaled to different values, and – naturally – more ragged. Indeed, we see anisotropy – ellipses with axes inclined roughly the same way in both figures. And, what is more important, we notice asymmetry in the rare events PDF. The left edge of the outer level corresponds to  $u'_r = -15.4$ , while the right edge of it is at  $u'_r = 13.8$ ; the left edge of the next level corresponds to  $u'_r = -10.7$ , while the right edge is at  $u'_r = 10.2$ .

If we characterize the asymmetry by the ratio of the distance from the left edge of the level to zero to the distance from the right edge of the level to zero, we will get for both figures 1 and 2 – for the external levels the number 1.1, while for the next levels (again for the both figures) the value of 1.05. Thus, approximately, the asymmetry is the same in both

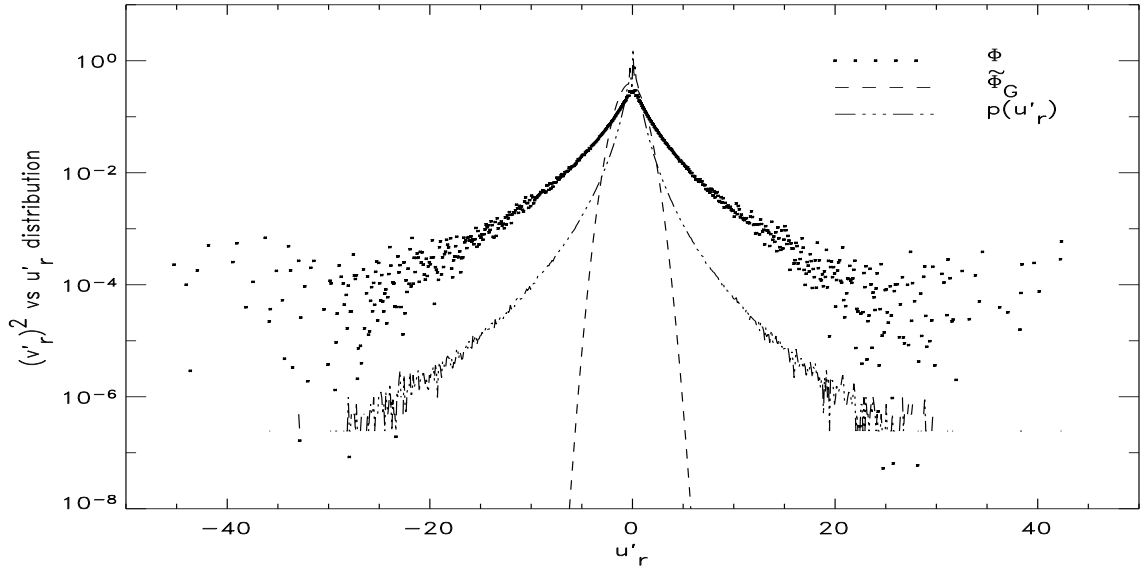


FIG. 3: Experimental  $v'_r{}^2$  distribution, compared with its Gaussian analog, and with  $p(u'_r)$ .

typical and rare events.

### THE $v'_r{}^2$ VERSUS $u'_r$ DISTRIBUTION: FUNCTION $\Phi$ , (7)

#### Global features

Figure 3 presents experimental  $v'_r{}^2$  versus  $u'_r$  distribution. It is compared with its Gaussian analog on one hand, and with regular experimental distribution  $p(u'_r)$  on the other. All three distributions in the figure are normalized on unity, i.e.,

$$\int \Phi(u'_r) du'_r = \int \tilde{\Phi}_G(u'_r) du'_r = \int p(u'_r) du'_r = 1,$$

and therefore their direct comparison makes sense.

It is clear that  $v'_r{}^2$ -distribution has quite extensive tails. Naturally, the Gaussian distribution is much lower outside its core part. Moreover, the tail parts of  $\Phi(u'_r)$  are much above corresponding parts of  $p(u'_r)$ . This is because the  $v'_r{}^2$ -distribution is a second moment, see definition (7), while  $p(u'_r)$  is a zeroth moment of the same distribution,

$$p(u'_r) = \int p(u'_r, v'_r) dv'_r.$$

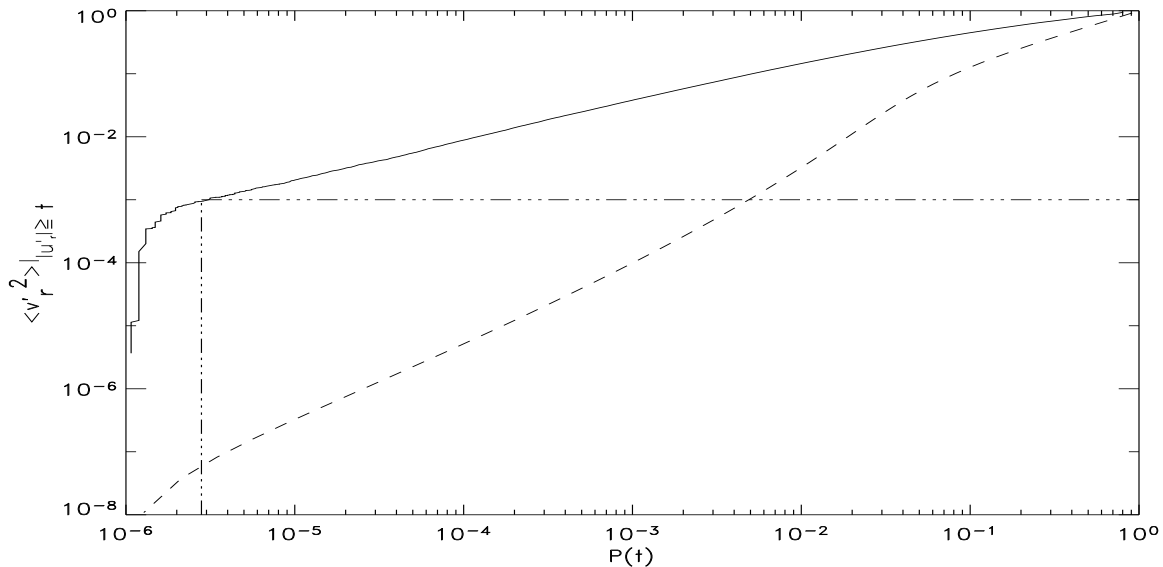


FIG. 4: Experimental  $v_r^2$ -distribution for  $|u_r| \geq t$  events versus the probability of these events  $P(t)$  (solid line), compared with its Gaussian counterpart (dashed line).

Note that the  $v_r^2$ -distribution is much more dispersed at the tail parts as compared with  $p(u_r)$  in the same areas. Analogous (huge) dispersion of data is observed in conditional average, see below Fig. 7, and is discussed in Subsection . We note here only that this dispersion is attributed to the presence of intermittency.

### Contribution of the rare violent events

Additional information about the tails of the  $v_r^2$  versus  $u_r$  distribution can be obtained from cumulative moments,

$$\langle v_r^2 \rangle_{|u_r| \geq t} = \int_{-\infty}^{-t} \Phi(u_r) du_r + \int_t^{\infty} \Phi(u_r) du_r, \quad (11)$$

that is, the contribution of events with  $|u_r| \geq t$  into the moment  $\langle v_r^2 \rangle$ , see definition of this moment in (10). These moments will be plotted against

$$P(t) = \int_{-\infty}^{-t} p(u_r) du_r + \int_t^{\infty} p(u_r) du_r, \quad (12)$$

the probabilities of these events.

Figure 4 presents such a plot. The experimental distribution is compared with its Gaussian counterpart. For  $t = 0$ , all events are presented, and therefore  $P(t = 0) = 1$  and  $\langle v_r'^2 \rangle \Big|_{|u_r'| \geq 0} = 1$ . If, on the other hand,  $t \rightarrow \infty$ , then both distributions go to zero.

The difference between experimental and Gaussian cases is quite substantial. As an example (depicted by dashed-dotted straight lines), we see that  $\langle v_r'^2 \rangle$  reaches  $10^{-3}$  fraction of its final value with only  $2.8 \times 10^{-6}$  part of all events. According to our estimate, these events correspond to quite violent outbursts with  $t \geq 27.4$  As seen from Fig. 3, these events are almost at the very end of the measured tails. The Gaussian counterpart reaches the same value of  $10^{-3}$  with  $4.7 \times 10^{-3}$  part of events; both these numbers are comparable for the Gaussian distribution.

On the other hand, the  $\langle v_r'^2 \rangle$  of the Gaussian counterpart with the same probability  $2.8 \times 10^{-6}$  as the experimental reaches only  $5.8 \times 10^{-8}$  fraction of its final value, these numbers being again more or less comparable.

### Asymmetry

Note that all three distributions depicted in Fig. 3 are constructed with the same resolution, that is, the bin-size for all three distribution was the same and equal to 0.1. This makes it possible to compare the dispersion of the data for different distributions. On the other hand, huge dispersion of the  $v_r'^2$ -distribution does not make it possible to compare its tails. In order to do this, we have to have a more smooth PDF, and that can be done by constructing the distribution with a larger bin-size. Figure 5 presents the  $v_r'^2$ -distribution constructed with a bin-size = 1.

Figure 5(a) compares the positive and negative parts of the distribution directly. It is obvious that the negative tail prevails over the positive for rather big  $u_r'$ . That is, the rare stormy events are definitely asymmetric.

The  $v_r'^2$ -distribution can be considered as a PDF centered at  $u_r' = k_a$ , see (9). That is, the distribution is definitely asymmetric, and theoretically, this asymmetry *should be* present at the tails as well. This actually can be seen from the shifted Gaussian distribution  $\tilde{\Phi}$ , see definition (18) and (22), and from the Fig. 5(a), that the negative part of the distribution is above the positive for any  $u_r'$ .

In order to see if the  $v_r'^2$ -distribution is just a shifted distribution, or not, we make direct

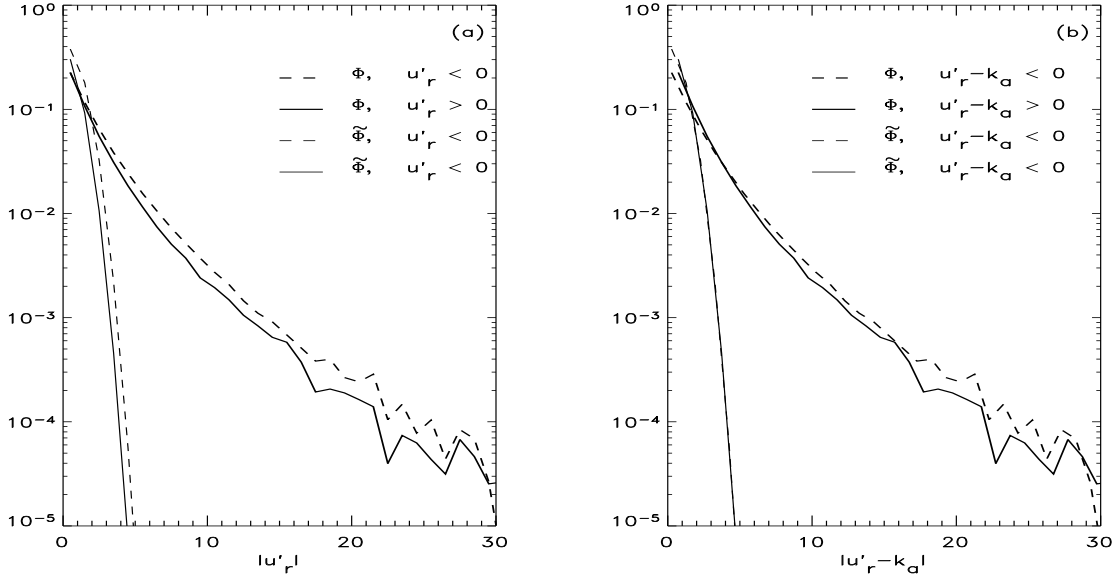


FIG. 5: Experimental  $v_r'^2$ -distribution. Direct comparison of the left and right wings.

comparison of its part where  $u_r' - k_a$  is positive with the part where  $u_r' - k_a$  is negative, see 5(b). The two parts of the corresponding Gaussian distribution  $\tilde{\Phi}$ , of course, coincide (and cannot be distinguished in the plot), while the experimental distribution still shows asymmetry: The centered negative part still prevails. This confirms the above conclusion that the rare violent events are asymmetric.

Another test for asymmetry is measuring the contribution of rare events, as in Subsection . Namely, we will consider cumulative moments,

$$\langle u_r v_r^2 \rangle \Big|_{|u_r| \geq t} = \int_{-\infty}^{-t} u_r \Phi(u_r) du_r + \int_t^{\infty} u_r \Phi(u_r) du_r, \quad (13)$$

cf. (11). Or, in dimensionless form,

$$k_a(t) = \langle u_r' v_r'^2 \rangle \Big|_{|u_r'| \geq t} = \int_{-\infty}^{-t} u_r' \Phi(u_r') du_r' + \int_t^{\infty} u_r' \Phi(u_r') du_r', \quad (14)$$

The case  $t = 0$  corresponds to all events, so that  $k_a(t = 0)$  assumes its final value, and at  $t > 0$  it approaches it. The case  $t \rightarrow \infty$  corresponds to  $k_a = 0$ . Figure 6 illustrates  $k_a(t)/k_a(0)$ , or actually it shows how the the third moment (9) is formed.

Obviously, there is a big difference between the experimental  $k_a(t)/k_a(0)$  and its Gaussian counterpart, as seen from Fig. 6. As an example (see the dashed-dotted straight lines in the

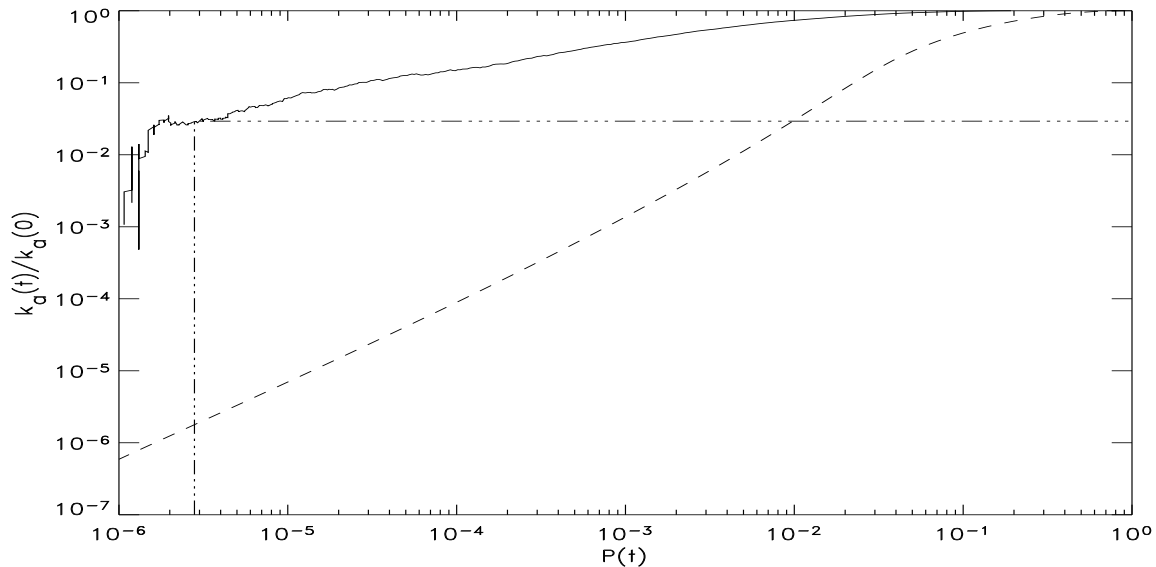


FIG. 6: Experimental  $k_a(t)$  (defined in (14)) for  $|u'_r| \geq t$  events versus the probability of these events  $P(t)$ .

figure), we took the same probability  $2.8 \times 10^{-6}$  as in Fig. 4, corresponding to extremely violent events. This time, it reaches 0.03th fraction of its final value. In contrast, its Gaussian counterpart reaches the same fraction with 0.01 part of events, – these two numbers (0.03 and 0.01) being comparable (cf. Subsection ). On the other hand, the Gaussian counterpart with probability  $2.8 \times 10^{-6}$  reaches the value of  $1.8 \times 10^{-6}$ . Again, these two numbers are comparable.

Thus, the contribution of the rare violent events into the experimental moment (9) is substantial, as opposed to the "regular" situation presumably illustrated by Gaussian distribution. Recall that this (odd) moment does not vanish due to asymmetry of the distributions, and therefore this substantial contribution of the rare violent events into  $k_a$ -moment means that these events also possess asymmetry.

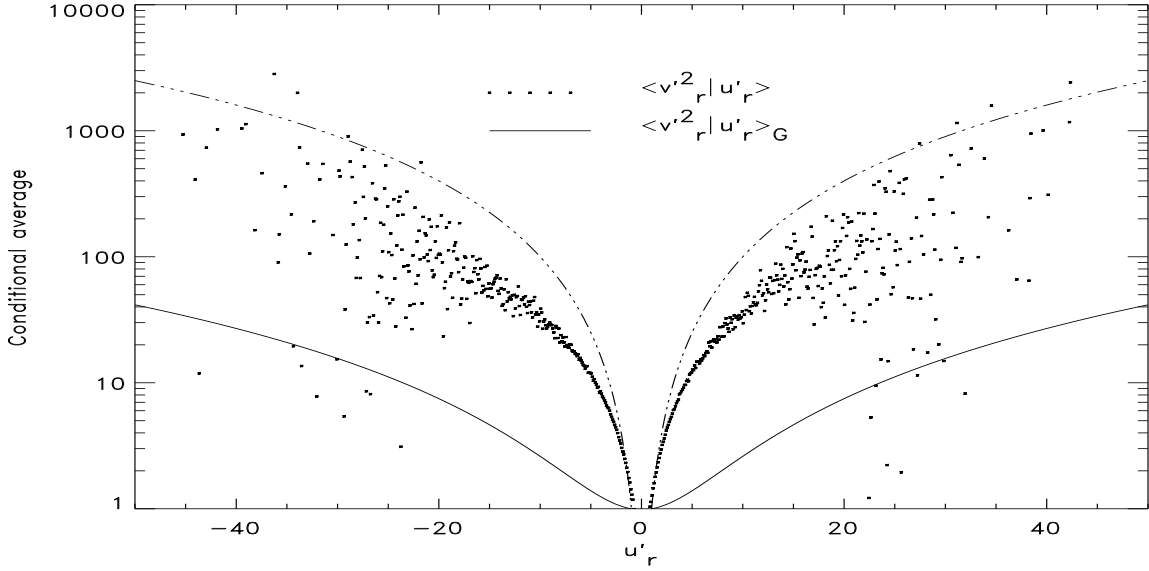


FIG. 7: Experimental conditional average  $\langle v_r'^2 | u_r' \rangle$ , compared with Gaussian defined in (21), and with "ideal" correlation, depicted by dashed-dotted line.

## CONDITIONAL AVERAGES

### Global properties

It is interesting to note that the the experimental conditional average  $\langle v_r'^2 | u_r' \rangle$  is much above the Gaussian defined in (21), see Fig. 7. If these two variables,  $u_r'$  and  $v_r'$  would be statistically independent, then the conditional average is unity, well below experimental average. The anisotropic Gaussian distribution (for which  $u_r'$  and  $v_r'$  variables are related, and therefore so are  $u_r'$  and  $v_r'^2$ ), is still much lower than experimental, as seen from the figure.

In another extreme case (as opposed to statistically independent variables) we have an "ideal" correlation,  $v_r' = \alpha u_r'$ , where  $\alpha$  is a constant, which is, due to our normalization, equal to unity. Then, simply,

$$\langle v_r'^2 | u_r' \rangle = u_r'^2$$

(cf. with Gaussian conditional average with maximal correlation coefficient  $C = \pm 1$ , from (21)). As seen from the Fig. 7, this conditional average is even higher than the experimental

value: Of course, any connection between two variables is less than "ideal".

Another remarkable feature of this average is its gigantic dispersion, cf. Subsection . Perhaps, the simplest way to explain it is to consider the two variables  $u'_r$  and  $v'_r$  statistically independent. As mentioned above, in this case, theoretically  $\langle v'^2_r | u'_r \rangle = 1$ . However, experimental measurements would give dispersed values, the statistics being defined by the number of events. To be more specific, for small and moderate values of  $|u'_r|$  with huge number of events, the data of  $\langle v'^2_r \rangle$  would be quite close to unity. For big values of  $|u'_r|$ , with only few events the data would be strongly dispersed around unity. In particular, if there is only one event in some bins, then the values of  $\langle v'^2_r \rangle$  would coincide with  $v'^2_r$  themselves, and they would be quite dispersed if the process is intermittent. Qualitatively, the experimental conditional average in the Fig. 7 looks as described above, that is, it is smooth for small and moderate values of  $|u'_r|$ , and strongly dispersed for big values. Returning to  $v'^2_r$  vs  $u'_r$  distribution, i.e., function  $\Phi(u'_r)$ , we recall that  $\Phi(u'_r) = \langle v'^2_r | u'_r \rangle p(u'_r)$ , see (6), where,  $p(u'_r)$  is not very dispersed function, as seen from Fig. 3. Therefore, the dispersion of the  $v'^2_r$  vs  $u'_r$  distribution is explained analogously to the dispersion of conditional average  $\langle v'^2_r | u'_r \rangle$ .

### Asymmetry

The data in Fig. 7 are presented with relatively high resolution, the bin-size being equal to 0.1. This makes it possible to see the dispersion and to interpret it as in Subsection . On the other hand, it is difficult to study the asymmetry with these dispersed data. Another processing of data with bin-size equal to 1 are presented in Fig. 8, where we compare the negative and positive parts of this conditional average directly.

We note here that Gaussian expression for conditional average (21) calculated from the joint 2D distribution (16) and used in Fig. 8 is symmetric (recall that it is not known how to include asymmetry into Gaussian or some other simple test 2D distribution). For this reason, the difference between the right and left Gaussian wings in both figures (a) and (b) is spurious. Still, putting the Gaussian conditional average into these two plots seems to be useful in order to compare the experimental data with something "regular".

Both quantities,  $\langle v'^2_r \rangle$  vs  $u'_r$  distribution, Fig. 5, and  $\langle v'^2_r | u'_r \rangle$ , Fig. 8, are related. For that reason in the latter figure we also check the symmetry in respect to the  $u'_r = k_a$  point (in 8(b), analogously to 5(b)), in addition to the symmetry in respect to  $u'_r = 0$  point, given

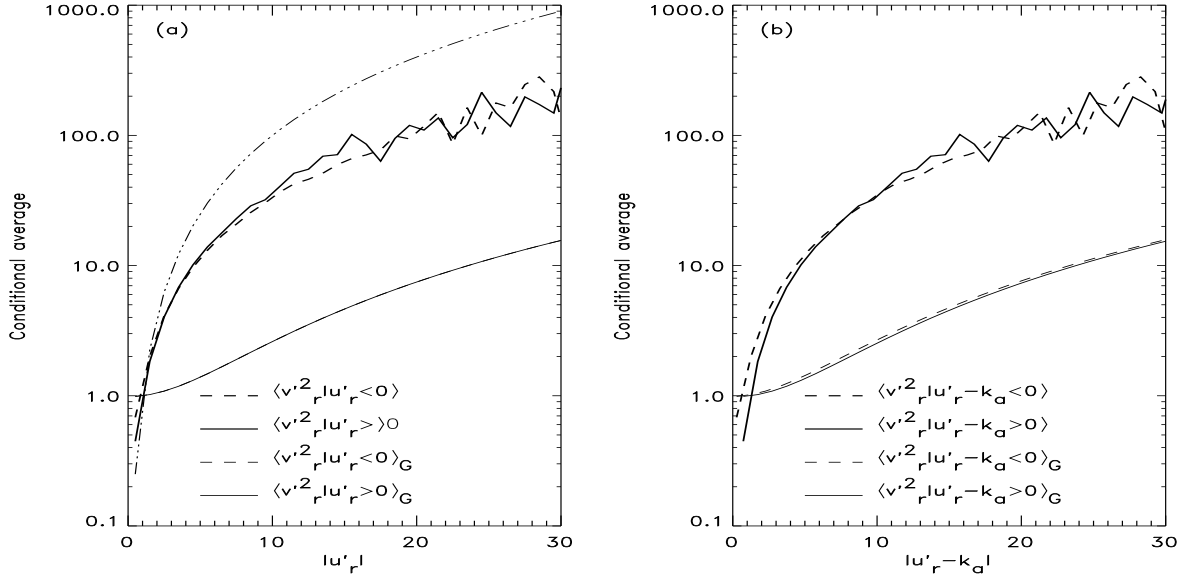


FIG. 8: Direct comparison of negative and positive parts of conditional average  $\langle v_r'^2 | u'_r \rangle$ . Dashed-dotted line corresponds to "ideal" correlation.

in 5(a) and 8(a). In other words, we check if the conditional average  $\langle v_r'^2 | u'_r \rangle$  is simply a shifted (but still symmetric) distribution, or not.

Close examination of Fig. 8 suggests that there is no substantial asymmetry *as a systematic trend* in this conditional average. Although this is an unexpected conclusion, there might be an explanation as follows. As can be seen from Fig. 5, the  $\langle v_r'^2 \rangle$  distribution, i.e., the function  $\Phi(u'_r)$ , is asymmetric, and so is the  $u'_r$  distribution,  $p(u'_r)$ , see [22]. This means that, in particular, the negative wings of both quantities are elevated above the right-hand wings. According to (6), the conditional average  $\langle v_r'^2 | u'_r \rangle$  is defined as a ratio of these two quantities. This suggests that increased value of  $\Phi(u'_r)$  in numerator is balanced by increased value of  $p(u'_r)$  in denominator, decreasing the asymmetry of  $\langle v_r'^2 | u'_r \rangle$ . In other words, the latter quantity appears to be less sensitive to the asymmetry than the former two.

## DISCUSSION

The asymmetry of turbulence has been studied for a long time. Its relation to the vorticity production was pointed out by [28]. The asymmetry of  $u_r$ -distribution resulting in the 4/5-Kolmogorov law was interpreted with the help of the ramp-model, see [17], [21]: As  $\langle u_r \rangle = 0$ , any compression, with  $u_r < 0$ , is as efficient as expansion, with  $u_r > 0$ . However, the compression appears stronger but rarer than decompression, the latter being weaker and longer. Therefore,  $\langle u_r^3 \rangle \neq 0$ . This model immediately suggests that this asymmetry is related to the intermittency: The compressed rare but strong events are supposed to be intermittent.

The ramp-model is only heuristic, however. It was shown by [29], [30], [31] that Burgers vortex, embedded into a converging motion, acquires negative skewness, this picture containing both asymmetry and intermittency. As the ramp-model does not exactly correspond to this picture, it had to be modified. This modification was called the bump-model, see [27]. Actually, “the bump” corresponds to the Burgers vortex. This model is now two-dimensional, – to include transverse velocity increments  $v_r$  into the picture. In particular, it automatically explains why the mixed third moment  $\langle u_r v_r^2 \rangle$ , (3), does not vanish.

Fully two-dimensional PDF describing all three items, namely asymmetry, anisotropy and intermittency, was discussed in this paper. The PDF, and also some additional conditional and cumulative averages seem to support the idea about the connection between these three features. In the whole picture, there is additional (to the Kolmogorov cascade) energy transport from the large non-universal scales directly to the small scales. We note that the Burgers vortex, with a small radius, is generated by a relatively large-scale motion, thus making it possible to transfer the energy directly from large scales to small. In the framework of the bump-model, it is “the bump” which is generated analogously to the Burgers vortex. The scale of the bump is definitely much smaller than the scale of the generating it motion (which can be seen from Fig. 5(c) by [27]), and that could explain the direct interaction between the non-universal large scales and small scales.

I thank K. R. Sreenivasan and S. Kurien for the data and for useful discussions.

## Appendix

The Gaussian joint PDF has the form,

$$p_G(u_r, v_r) = \frac{1}{2\pi\sqrt{\langle u_r^2 \rangle \langle v_r^2 \rangle - \langle u_r v_r \rangle^2}} \exp \left\{ -\frac{u_r^2 \langle v_r^2 \rangle - 2u_r v_r \langle u_r v_r \rangle + v_r^2 \langle u_r^2 \rangle}{2(\langle u_r^2 \rangle \langle v_r^2 \rangle - \langle u_r v_r \rangle^2)} \right\}, \quad (15)$$

$\langle u_r \rangle = \langle v_r \rangle = 0$ . Or, for dimensionless variables,

$$p_G(u'_r, v'_r) = \frac{1}{2\pi\sqrt{1-C^2}} \exp \left\{ -\frac{u'^2_r - 2u'_r v'_r C + v'^2_r}{2(1-C^2)} \right\} \quad (16)$$

where

$$C = \langle u'_r v'_r \rangle = \frac{\langle u_r v_r \rangle}{\langle u_r^2 \rangle^{1/2} \langle v_r^2 \rangle^{1/2}}, \quad (17)$$

the correlation coefficient. Note that in isotropic turbulence  $C$  vanishes, and therefore the distribution (15), or (16), corresponds to anisotropic Gaussian process. Note, however, that this distribution is not asymmetric. Indeed, it is easy to show that  $\langle u_r^3 \rangle_G = \int u_r^3 p_G(u_r, v_r) du_r dv_r = 0$  and  $\langle u_r v_r^2 \rangle_G = \int u_r v_r^2 p_G(u_r, v_r) du_r dv_r = 0$ .

For Gaussian distribution (15),

$$\Phi_G(u_r) = \frac{1}{\sqrt{2\pi}} \left[ \frac{\langle u_r^2 \rangle \langle v_r^2 \rangle - \langle u_r v_r \rangle^2}{\langle u_r^2 \rangle^{3/2}} + u_r^2 \frac{\langle u_r v_r \rangle^2}{\langle u_r^2 \rangle^{5/2}} \right] \exp \left\{ -\frac{u_r^2}{2\langle u_r^2 \rangle} \right\} \quad (18)$$

Or, for dimensionless variables, we have,

$$\Phi_G(u'_r) = \frac{1}{\sqrt{2\pi}} [1 - C^2 + u'^2_r C^2] \exp \left\{ -\frac{u'^2_r}{2} \right\} \quad (19)$$

For Gaussian distribution, according to (5) and (18), we have

$$\langle v_r^2 | u_r \rangle_G = \langle v_r^2 \rangle \left[ 1 - C^2 + \frac{u_r^2}{\langle u_r^2 \rangle} C^2 \right], \quad (20)$$

or

$$\langle v'^2_r | u'_r \rangle_G = 1 - C^2 + u'^2_r C^2 \quad (21)$$

These Gaussian expressions are useful to check in two limiting cases. If  $C = 0$ , the two variables  $u_r$  and  $v_r$  become statistically independent, and, naturally,  $\langle v_r^2 | u_r \rangle = \langle v_r^2 \rangle$ . In another limiting case of perfect correlation,  $v_r = \alpha u_r$ , and therefore  $C = \pm 1$ , then  $\langle v_r^2 | u_r \rangle = \alpha^2 u_r^2 = \langle v_r^2 \rangle u_r^2 / \langle u_r^2 \rangle$ . These two extreme cases are indeed confirmed by (20).

As mentioned above, the Gaussian distribution (15) is not asymmetric. It is not known how to construct a simple test 2D PDF containing both anisotropy and asymmetry. We

therefore are going to use (15) directly comparing it with the experimental joint 2D PDF. However, in all expressions containing 1D PDF, instead of symmetric 1D PDF resulting from integration of the PDF (16) over  $dv'_r$ , we will use a simple asymmetric PDF,  $I_r$ , constructed as a sum of two Gaussian distributions, see [22] and [27], so that

$$\int I_r du'_r = 1, \quad \int u'_r I_r du'_r = \langle u'_r \rangle = 0, \quad \int u'^2_r I_r du'_r = \langle u'^2_r \rangle = 1, \quad \text{and} \quad \int u'^3_r I_r du'_r = \langle u'^3_r \rangle.$$

Being asymmetric it is otherwise almost indistinguishable from Gaussian 1D PDF following from (16), at least visually.

The Gaussian  $\Phi_G(x)$  should be "corrected" as well to incorporate asymmetry. We will therefore use

$$\tilde{\Phi}_G(x') = \Phi_G(x' - k_a), \tag{22}$$

instead of  $\Phi_G(x)$  defined in (18). Then, of course,

$$\langle u'_r v'^2_r \rangle_G = \int u'_r \tilde{\Phi}_G(u'_r) du'_r = k_a.$$

Note that the difference between the plots of  $\Phi_G$  and  $\tilde{\Phi}_G$  is only cosmetic.

- 
- [1] A. N. Kolmogorov, C.R. Acad. Sci. U.S.S.R. **30**, 301 (1941).
- [2] S. Tavoularis and S. Corrsin, J. Fluid Mech. **104**, 311 (1981).
- [3] K. R. Sreenivasan, Proc. Roy. Soc. Lond. A **434**, 165 (1991).
- [4] X. Shen and Z. Warhaft, Phys. Fluids **12**, 2976 (2000).
- [5] M. Ferchichi and S. Tavoularis, Phys. Fluids **12**, 2942 (2000).
- [6] Z. Warhaft and X. Shen, Physics of Fluids **14**, 2432 (2002).
- [7] J. Schumacher, K. R. Sreenivasan, and P. K. Yeung, Phys. Fluids **15**, 84 (2003).
- [8] A. Staicu, B. Vorselaars, and W. van de Water, Phys. Rev. E **68** (2003).
- [9] K. R. Sreenivasan and B. Dhruva, Progress of Theoretical Physics Supplement **No. 130**, 103 (1998).
- [10] S. Kurien and K. R. Sreenivasan, Phys. Rev. E **62**, 2206 (2000).
- [11] L. Biferale and F. Toschi, Phys. Rev. Lett. **86**, 4831 (2001).
- [12] L. Biferale and I. Procaccia, Phys. Rep. **414**, 43 (2005).
- [13] S. Kurien, Physica D **175**, 167 (2003).
- [14] L. Biferale and M. Vergassola, Phys. Fluids **13**, 2139 (2001).
- [15] A. Pumir and B. I. Shraiman, Phys. Rev. Lett. **75**, 3114 (1995).
- [16] A. Staicu and W. van de Water, Phys. Rev. Lett. **90** (2003).
- [17] S. I. Vainshtein and K. R. Sreenivasan, Phys. Rev. Lett. **73**, 3085 (1994).
- [18] A. N. Kolmogorov, C.R. Acad. Sci. U.S.S.R. **32**, 16 (1941).
- [19] L. D. Landau and E. M. Lifschitz, *Fluid Mechanics* (Pergamon Press, Oxford, 1987).
- [20] A. S. Monin and A. M. Yaglom, *Statistical Fluid Mechanics*, vol. 2 (MIT Press, Cambridge, Mass., 1971).
- [21] K. R. Sreenivasan, S. I. Vainshtein, R. Bhiladvala, I. San Gil, S. Chen, and N. Cao, Phys. Rev. Lett. **77**, 1488 (1996).
- [22] S. I. Vainshtein, Phys. Rev. E **61**, 5228 (2000).
- [23] J. L. Lumley, Phys. Fluids **10**, 855 (1967).
- [24] K. R. Sreenivasan and R. A. Antonia, AIAA J. **16**, 867 (1978).
- [25] K. R. Sreenivasan, R. A. Antonia, and S. E. Stephenson, AIAA J. **16**, 869 (1978).
- [26] C. Meneveau, K. R. Sreenivasan, P. Kailasnath, and M. S. Fan, Phys. Rev. A **41**, 894 (1990).

- [27] S. I. Vainshtein, *J. Fluid Mech.* **558**, 243 (2006).
- [28] R. Betchov, *J. Fluid Mech.* **1**, 497 (1956).
- [29] J. Jiménez, *Phys. Fluids A* **4**, 652 (1992).
- [30] N. Hatakeyama and T. Kambe, *Phys. Rev. Letters* **79**, 1257 (1997).
- [31] M. Tanaka and S. Kida, *Phys. Fluids A* **5**, 2079 (1993).